Space Mapping Optimization of Waveguide Filters Using Finite Element and Mode-Matching Electromagnetic Simulators*

John W. Bandler,[1†] Radoslaw M. Biernacki,[2] Shao Hua Chen,[2] Dževat Omeragić[3]

[1]Simulation Optimization Systems Research Laboratory and Department of Electrical and Computer Engineering, McMaster University, Hamilton, Canada L8S 4L7
[2]HP EEsof Division, Hewlett-Packard Company, 1400 Fountaingrove Parkway, Santa Rosa, California 95403-1799
[3]Formation Evaluation Department, Schlumberger Oilfield Services, P.O. Box 2175, MD-5, Houston, Texas 77252-2175

ABSTRACT: For the first time in design optimization of microwave circuits, the aggressive space mapping (SM) optimization technique is applied to automatically align electromagnetic (EM) models based on hybrid mode-matching / network theory simulations with models based on finite-element (FEM) simulations. SM optimization of an *H*-plane resonator filter with rounded corners illustrates the advantages as well as the challenges of the approach. The parameter extraction phase of SM is given special attention. The impact of selecting responses and error functions on the convergence and uniqueness of parameter extraction is discussed. A statistical approach to parameter extraction involving l_1 and penalty concepts facilitates a key requirement by SM for uniqueness and consistency. A multipoint parameter extraction approach to sharpening the solution uniqueness and improving the SM convergence is also introduced. Once the mapping is established, the effects of manufacturing tolerances are rapidly estimated with the FEM accuracy. SM has also been successfully applied to optimize waveguide transformers using two hybrid mode-matching / network theory models: a coarse model using very few modes and a fine model using many modes to represent discontinuities. © 1999 John Wiley & Sons, Inc. Int J RF and Microwave CAE 9: 54–70, 1999.

Keywords: optimization techniques; space mapping

I. INTRODUCTION

Direct exploitation of electromagnetic (EM) simulators in the optimization of arbitrarily shaped 3D structures at high frequencies is crucial for first-pass success CAD [1, 2]. Recently, we reported successful automated design optimization of 3D structures using FEM simulations [1, 3].

The objective of space mapping (SM) [3–5] is to avoid direct optimization of computationally intensive models. In this article, for the first time, aggressive space mapping (ASM) optimization is applied to automatically align the results of two separate EM simulation systems. The RWGMM library [6, 7] of waveguide models based on the mode matching (MM) technique [6–8] is used for

Correspondence to: John W. Bandler
*All authors were formerly affiliated with the Simulation Optimization Systems Research Laboratory and the Department of Electrical and Computer Engineering, McMaster University, Hamilton, Ontario, Canada L8S 4L7, and with Optimization Systems Associates Inc., Dundas, Ontario, Canada, before acquisition by HP EEsof.
†Also affiliated with Bandler Corporation, P.O. Box 8083, Dundas, Ontario, Canada L9H 5E7.

CCC 1096-4290/99/010054-17

fast/coarse simulations in the so-called optimization space X_{os}. The library is linked to the network theory optimizers of OSA90/hope™ (Hewlett-Packard, Santa Rosa, CA). Ansoft's Maxwell Eminence (Ansoft, Pittsburgh, PA) or HP HFSS (Hewlett-Packard, Santa Rosa, CA) (both widely known simply as HFSS) simulations accessed through Empipe3D™ (Hewlett-Packard, Santa Rosa, CA) serve as the "fine" model in the so-called X_{em} space. The SM procedure executes all these systems concurrently.

Both RWGMM and HFSS provide accurate EM analysis. RWGMM is computationally efficient in its treatment of a variety of predefined geometries. It is ideally suited for modeling complex waveguide structures that can be decomposed into the available library building blocks. FEM-based simulators [9, 10] such as HFSS are able to analyze arbitrary shapes, but they are computationally very intensive.

ASM optimization of an H-plane resonator filter with rounded corners is carried out. These rounded corners make RWGMM simulations somewhat less accurate. Once the mapping is established, subsequent Monte Carlo analysis of manufacturing tolerances exploits the FEM-based space-mapped model with the speed of the MM/network theory simulator. To illustrate the flexibility in selecting the X_{em} and X_{os} models, SM is also applied to optimize waveguide transformers using two hybrid MM/network theory models: a coarse model using very few modes and a fine model using many modes to represent the discontinuities.

The parameter extraction phase is the key to effective SM optimization. The methodology, however, is sensitive to nonunique solutions or local minima inconsistent with the desired solution. An in-depth study of this phenomenon is presented and ways to overcome such problems are addressed. We show that, at the expense of increased simulations of the fast coarse model, we can satisfy the requirement for uniqueness and consistency. We investigate how the choice of error functions influences the convergence and uniqueness of parameter extraction. We offer a solution based on statistical parameter extraction involving a powerful l_1 algorithm and penalty function concepts. We introduce a multipoint parameter extraction approach to sharpening the solution uniqueness and improving the SM convergence in the automated design of a waveguide transformer.

II. FULLY AUTOMATED SPACE MAPPING OPTIMIZATION

By inspecting the steps involved in SM optimization [4, 5], we recognize that the parameter extraction process is explicitly dependent on the specific models involved. In the flow diagram shown in Figure 1 the MM waveguide library serves as the X_{os} model and the FEM simulator serves as the X_{em} model. SM optimization starts with conventional design optimization of the coarse model: MM optimization, which leads to the optimal parameter values x_{os}^*. Those parameter values determine the starting point for the SM update loop, which can be implemented within a generic layer of iterations. Following this guideline, the ASM strategy has been fully automated using a two-level Datapipe architecture [11]. Figure 1 illustrates the two iterative loops involving two different sets of variables. The outer loop updates the optimization variables x_{em} of the X_{em} model based on the latest mapping. Within each SM iteration the inner, dotted block, extracts the parameters x_{os} of the X_{os} model while x_{em} is held constant. The parameter extraction process is carried out through auxiliary optimization iterations performed exclusively within the X_{os} model. The goal of parameter extraction is to

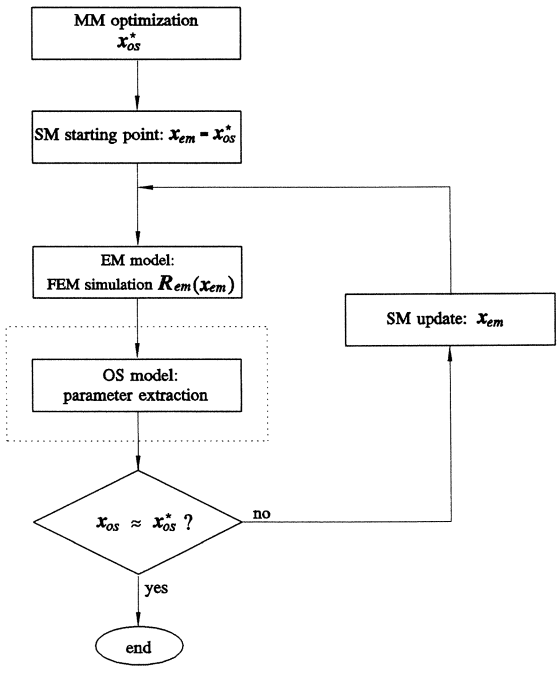

Figure 1. Flow diagram of the SM optimization procedure concurrently exploiting the hybrid MM/network theory and FEM techniques and statistical parameter extraction.

match the reference data: the fine model responses $\boldsymbol{R}_{em}(\boldsymbol{x}_{em})$ obtained from FEM simulation. The outer SM iterations terminate when the coarse model parameters $\boldsymbol{x}_{os}$ approach $\boldsymbol{x}_{os}^*$. The Datapipe techniques allow us to carry out the nested optimization loops in two separate processes while maintaining a functional link between their results (e.g., the next increment to $\boldsymbol{x}_{em}$ is a function of the results of parameter extraction).

Within the inner loop of parameter extraction, we can also utilize the Datapipe technique to connect external model simulators to the optimization environment (e.g., the Empipe3D system is a specialized Datapipe interface to HFSS). Further details of the parameter extraction step will be elaborated in Sections IV through VII.

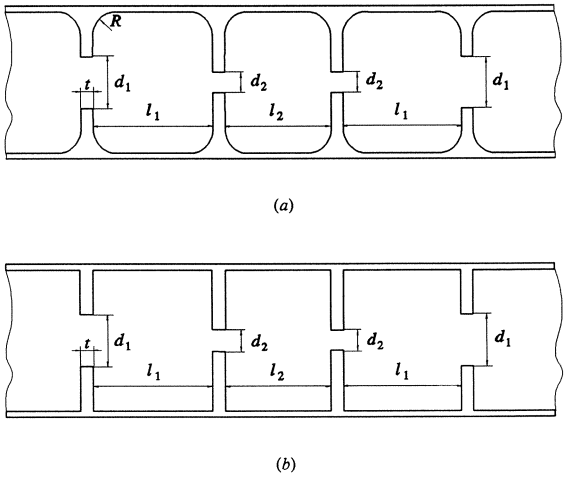

Figure 2. Structures for SM optimization: (a) X_{em} model, for analysis by FEM; (b) X_{os} model, for hybrid MM/network theory. The waveguide cross-section is 15.8 × 7.9 mm; the thickness of the irises is t = 0.4 mm. Optimization variables are iris openings d_1, d_2 and resonator lengths l_1, l_2.

III. SPACE MAPPING OPTIMIZATION USING MM / NETWORK THEORY AND FEM

We address the design of the H-plane resonator filter with rounded corners shown in Figure 2a. The waveguide cross-section is 15.8 × 7.9 mm, while the thickness of the irises is t = 0.4 mm. The radius of the corners is R = 1 mm. The iris and resonator dimensions d_1, d_2, l_1, and l_2 are selected as the optimization variables.

First, minimax optimization of the X_{os} model (Fig. 2b) is performed by exploiting the waveguide MM library with specifications provided by Arndt [12],

$$|S_{21}| < -35 \text{ dB} \quad \text{for } 13.5 \text{ GHz} \le f \le 13.6 \text{ GHz},$$
$$|S_{11}| < -20 \text{ dB} \quad \text{for } 14.0 \text{ GHz} \le f \le 14.2 \text{ GHz},$$
$$|S_{21}| < -35 \text{ dB} \quad \text{for } 14.6 \text{ GHz} \le f \le 14.8 \text{ GHz},$$

where f represents the frequency.

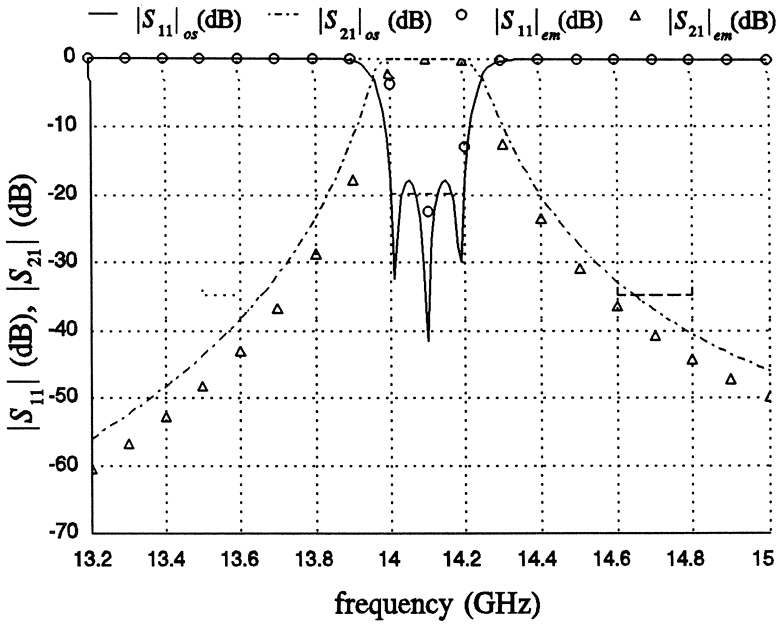

Figure 3. Magnitudes of S_{11} and S_{21} of the H-plane filter before SM optimization, as simulated using RWGMM (curves) and HFSS (points).

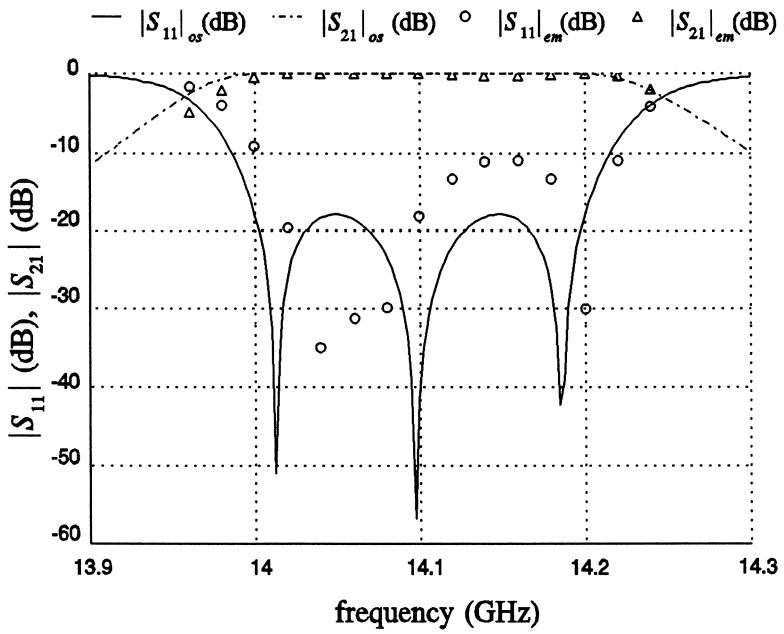

Figure 4. Magnitudes of S_{11} and S_{21} of the H-plane filter before SM optimization, as simulated using RWGMM (curves) and HFSS (points); passband detail.

The minimax solution $\boldsymbol{x}_{os}^*$ is $d_1 = 6.04541$, $d_2 = 3.21811$, $l_1 = 13.0688$, and $l_2 = 13.8841$. It yields the target response for SM. At this point, the fine model $\boldsymbol{X}_{em}$ is analyzed by FEM using the $\boldsymbol{x}_{os}^*$ values. The corresponding responses of the FEM model and hybrid mode-matching/network theory models are shown in Figure 3. Focusing on the passband, we treat responses in the region $13.96 \leq f \leq 14.24$ GHz. The passband responses of both models at the point $\boldsymbol{x}_{os}^*$ are shown in Figure 4. Some discrepancy is evident.

Tables I and II summarize the steps of the successful ASM optimization. The solution, corresponding to point $d_1 = 6.17557$, $d_2 = 3.29058$, $l_1 = 13.0282$, and $l_2 = 13.8841$, shown in Figure 5 was obtained after only four HFSS simulations, each with only 15 frequency points. The SM results were verified by directly optimizing the H-plane filter using Empipe3D driving the HFSS solver. Essentially the same solution was found.

TABLE I. Space Mapping Optimization of the H-Plane Filter[a]

Point	d_1	d_2	l_1	l_2
$\boldsymbol{x}_{em}^1$	6.04541	3.21811	13.0688	13.8841
$\boldsymbol{x}_{em}^2$	6.19267	3.32269	12.9876	13.8752
$\boldsymbol{x}_{em}^3$	6.17017	3.29692	13.0536	13.8812
$\boldsymbol{x}_{em}^4$	6.17557	3.29058	13.0282	13.8841

[a] Values of all optimization variables are in millimeters.

IV. ERROR FUNCTIONS FOR PARAMETER EXTRACTION

A natural choice in formulating the objective function for the parameter extraction phase of

TABLE II. Parameter Extraction Results for Space Mapping Optimization[a]

Point	d_1	d_2	l_1	l_2	$\|\boldsymbol{x}_{os}^* - \boldsymbol{x}_{os}^i\|$
$\boldsymbol{x}_{os}^1$	5.89815	3.11353	13.1500	13.8930	0.19823
$\boldsymbol{x}_{os}^2$	6.07714	3.25445	12.9757	13.8757	0.10519
$\boldsymbol{x}_{os}^3$	6.03531	3.22421	13.1119	13.8806	0.04482
$\boldsymbol{x}_{os}^4$	6.04634	3.22042	13.0618	13.8831	0.00750

[a] Values of all optimization variables are in millimeters.

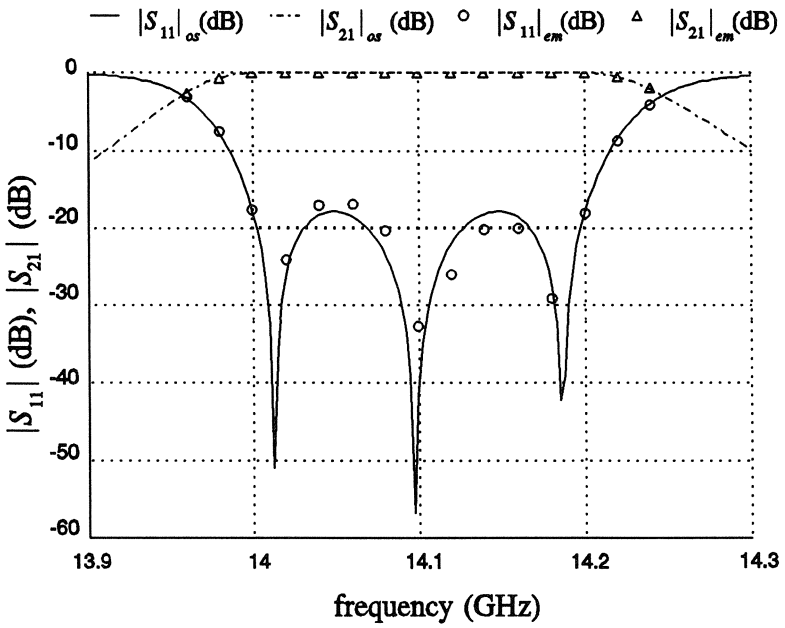

Figure 5. FEM responses (points) of the H-plane filter at the SM solution compared with optimal X_{os} target responses (curves). The results were obtained after only four simulations by HFSS.

SM is to use the responses for which the specifications are given. In the case of the H-plane filter, they are $|S_{11}|$ in decibels at selected passband frequencies, and thus the individual errors could be formed by subtracting $|S_{11}|$ in decibels from the corresponding specifications (also in decibels). A good choice of the objective function for parameter extraction is the ℓ_1 norm of the error vector. We are, however, free to use any error formulation that allows us to align the models. The results reported in the preceding section were obtained using $|S_{21}|$. With that formulation, the SM iterations proceeded flawlessly. No difficulty in the parameter extraction phase was noticed.

We also took a close look at the ℓ_1 objective function using some other error formulations. Figure 6 shows two cases of the ℓ_1 norm for parameter extraction during the second iteration of SM. They are determined in the vicinity of the starting point w.r.t. two selected parameters: the iris openings d_1 and d_2. Figure 6a corresponds to the error definition in terms of $|S_{11}|$ (dB). It exhibits many local minima and provides us with an excellent opportunity to investigate the uniqueness of the parameter extraction phase in SM, as well as to improve its robustness. When the errors are defined in terms of $|S_{21}|$ (as was used to obtain the SM results reported in Section III), the corresponding function surface becomes significantly smoother, as shown in Figure 6b.

V. STATISTICAL PARAMETER EXTRACTION

We propose an automated statistical parameter extraction procedure to overcome potential pitfalls arising out of inaccurate or nonunique solutions. First, we perform standard ℓ_1 parameter extraction [13] of the X_{os} model starting from x_{os}^*. If the resulting response matches well the X_{em} model response (the ℓ_1 error is small enough), we continue with the SM iterations. Otherwise, we turn to statistical exploration of the X_{os} model.

The key to statistical parameter extraction is to establish the exploration region. Unlike general purpose random/global optimization approaches, we want to carry out local statistical exploration as deemed suitable for SM. To this end, we take advantage of the fact that during the SM iterations the desired parameter extraction solutions should rapidly approach x_{os}^* in the X_{os} space (see [5, 14]).

Consider the kth SM iteration. When the current mapping $[x_{os} = P^{(k-1)}(x_{em})]$ is applied to the current point in the X_{em} model space, we arrive at x_{os}^*, since that point has been deter-

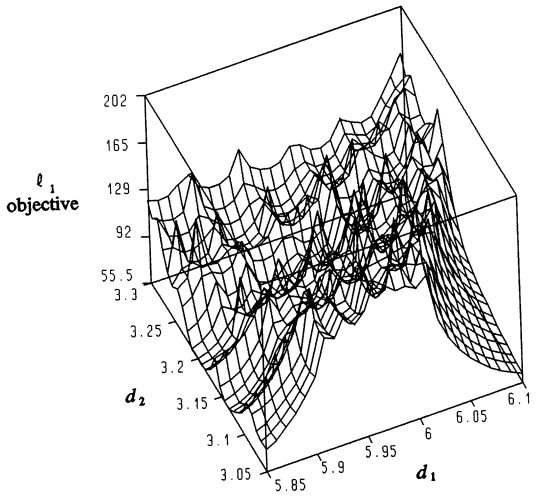

(*a*)

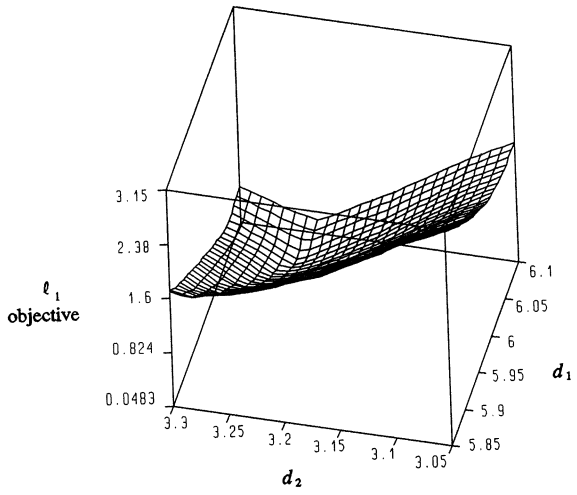

(*b*)

Figure 6. Variation of the ℓ_1 objective w.r.t. iris openings d_1 and d_2. Other parameters are held fixed at values corresponding to $\boldsymbol{x}_{os}^*$. Individual errors defined in terms of (a) $|S_{11}|$ (dB); (b) $|S_{21}|$.

mined by the inverse mapping $[\boldsymbol{x}_{em}^k = P^{(k-1)^{-1}}(\boldsymbol{x}_{os}^*)$; see [5]). The fact that the new point (to be extracted) differs from $\boldsymbol{x}_{os}^*$ is not only a basis for modifying the mapping, but also quantitatively establishes the degree of inconsistency w.r.t. the existing mapping. This allows us to define an appropriate exploration region. If, for the kth step, we define the multidimensional interval $\boldsymbol{\delta}$ as

$$\boldsymbol{\delta} = \boldsymbol{x}_{\text{os}}^{k-1} - \boldsymbol{x}_{\text{os}}^*, \tag{1}$$

the statistical exploration may be limited to the region defined by

$$x_{osi} \in [x_{osi}^* - 2|\delta_i|, x_{osi}^* + 2|\delta_i|]. \tag{2}$$

Another choice for the exploration region could be an elliptical multidimensional domain with semiaxes $2|\delta_i|$ defined by

$$\sum_i (x_{osi} - x_{osi}^*)^2/|\delta_i|^2 \leq 4. \tag{3}$$

A set of N_s starting points is then statistically generated within the region (2) or (3), and N_s parameter extraction optimizations are carried out. These parameter extractions are further aided by a penalty function [14] of the form

$$\lambda \|\boldsymbol{x}_{os}^k - \boldsymbol{x}_{os}^*\|, \tag{4}$$

which augments the ℓ_1 objective function. In the case of multiple minima, this penalty term forces the optimizer to select local minima closer to $\boldsymbol{x}_{os}^*$. The resulting solutions (expected to be multiple) are then categorized into clusters and ranked according to the achieved values of the error function. Finally, the penalty term is removed and the process is repeated to focus the clustered

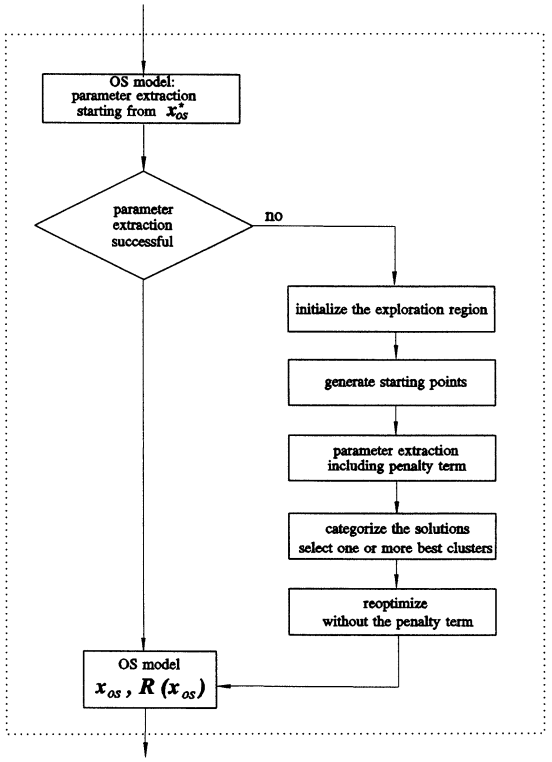

Figure 7. Flow diagram of the statistical parameter extraction procedure.

solution(s). Absence of the penalty term brings the solution point to the "true" local minimum, thus removing "fuzziness" that may occur when the penalty term is used. The aforementioned steps are briefly summarized by the following algorithm and are illustrated in the flow chart shown in Figure 7.

Algorithm

Step 1. Initialize the exploration region. Equation (2) or (3) can be used in the second and all subsequent SM iterations.
Step 2. Generate N_s random starting points.
Step 3. Perform N_s parameter extractions from the N_s starting points including the penalty function (4).
Step 4. Categorize the solutions. Select one or more best clusters of the solutions.
Step 5. Focus the clusters by reoptimizing without the penalty term.

This approach has been automated by adding one more level in the Datapipe architecture described in Section II. Furthermore, it can be parallelized, because the N_s parameter extractions considered are carried out independently.

VI. PARAMETER EXTRACTION OF THE *H*-PLANE FILTER

We use the *H*-plane filter example to investigate the statistical parameter extraction outlined in the preceding section. To verify the robustness of the approach, we have used the ℓ_1 objective function with various definitions of individual er-

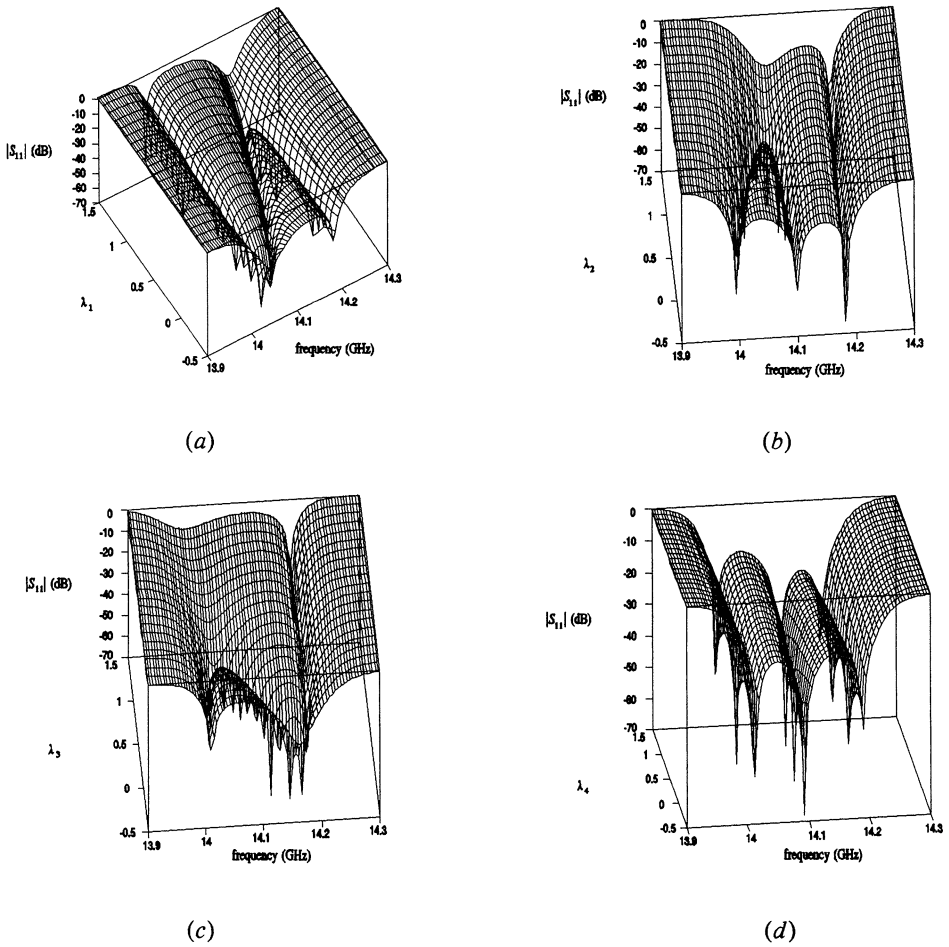

Figure 8. Three-dimensional plots of $|S_{11}|$ in decibels versus frequency and filter parameters: (a) opening of the first iris d_1; (b) opening of the second iris, d_2; (c) length of the first resonator; (d) length of the second resonator. The range of parameter changes is defined by the first SM step: $\lambda_i = 0$ at $\boldsymbol{x}_{os}^{*}$ and $\lambda_i = 1$ at $\boldsymbol{x}_{os}^{1}$.

rors. The case when the individual errors are defined in terms of $|S_{11}|$ in decibels was already illustrated by Figure 6a for the second iteration of ASM.

Figure 8 presents the variation of the MM/network theory model response in the vicinity of the starting point. Responses are computed along the direction of the first ASM step, defined by points $\boldsymbol{x}_{os}^{*}$ and $\boldsymbol{x}_{os}^{1}$. Although the responses shown in Figure 8 are all smooth when only one parameter is varied, the ℓ_1 objective function defined in terms of $|S_{11}|$ (dB) has multiple minima; hence, the optimizer may terminate at an undesirable solution.

A set of 100 starting points is statistically generated from a uniform distribution within the range (2). The distances between the point $\boldsymbol{x}_{os}^{*}$ and the random starting points are depicted in Figure 9a. The corresponding 100 ℓ_1 parameter extraction optimizations with the penalty term (4) are then performed from these points. The distances between $\boldsymbol{x}_{os}^{*}$ and the solutions of parameter extraction optimizations based on the errors defined in terms of $|S_{11}|$ in decibels are shown in Figure 9b. The solutions are scattered, confirming our observation that the ℓ_1 objective function has many local minima, as illustrated in Figure 6a. Among the 100 solutions, a cluster of 15 points is detected. Figure 9b provides some insight into the process of cluster selection: all the points within the cluster exhibit a similar distance from $\boldsymbol{x}_{os}^{*}$. A deciding factor, however, for a point to belong to the cluster is its distance from other points in the cluster. Therefore, only a subset of all the points with similar bar sizes can actually form the cluster. Furthermore, depending on the cluster "diameter," some points actually selected for the cluster may appear in Figure 9b as outliers. Once the cluster is identified, removing the penalty term and restarting the parameter extraction process from all its points further sharpens the solution. Here, all the points within the cluster converge to the same solution, as depicted in Figure 9c. Figures 10 and 11 show the responses of the $\boldsymbol{X}_{os}$ model at those 100 points before and after parameter extraction, respectively. Figure 12 displays the responses corresponding to the cluster of 15 points that converged to the same solution, validating successful parameter extraction.

Figure 13 illustrates the impact of the penalty term. When the penalty term is not used, only 10 parameter extractions lead to the desired solution, as shown in Figure 13a. Here $|S_{11}|$ in decibels is used to define the errors. Figure 13b and 13c presents the results when the errors are defined in terms of $|S_{21}|$. Without the penalty term, the procedure leads to 52 successful parameter extractions (Fig. 13a); adding the penalty term (4)

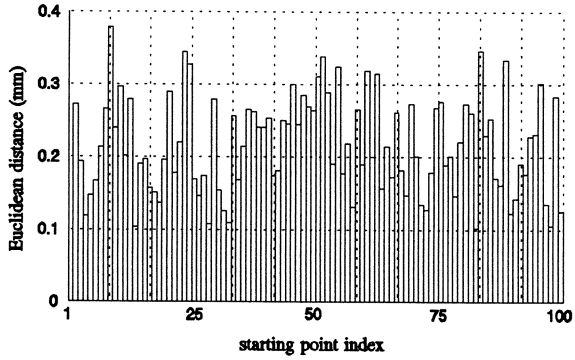

(*a*)

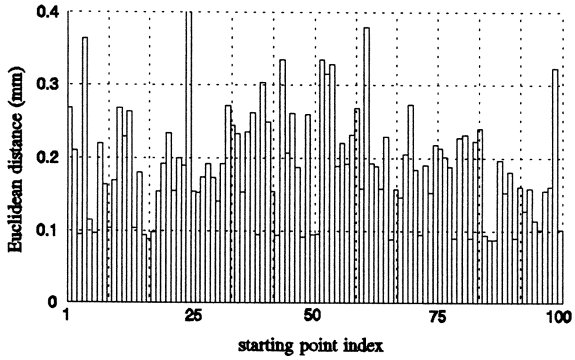

(*b*)

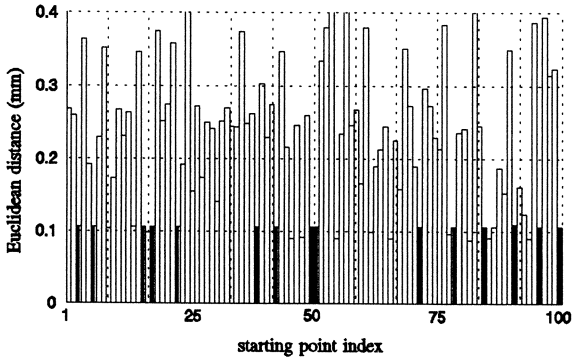

(*c*)

Figure 9. Euclidean distances measured from $\boldsymbol{x}_{os}^{*}$ to (a) the randomly generated starting points for statistical exploration, (b) the converged points after the first stage, and (c) the converged points after the second stage of statistical parameter extraction. Individual errors defined in terms of $|S_{11}|$ in decibels.

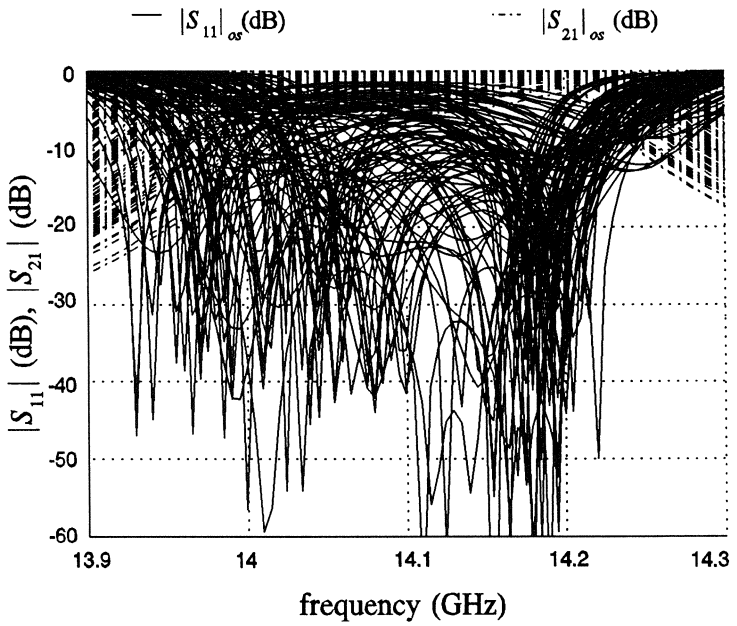

Figure 10. Statistical parameter extraction: responses at 100 randomly generated starting points.

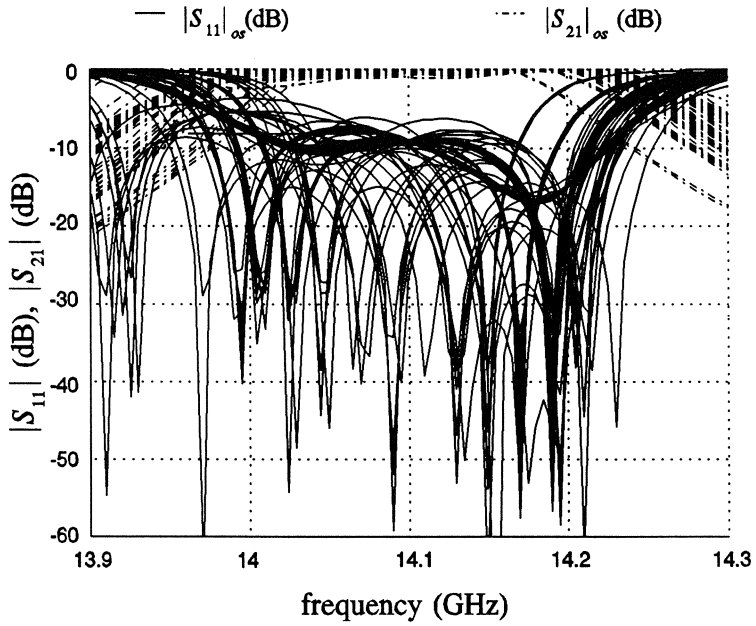

Figure 11. Statistical parameter extraction: responses at 100 solution points (after two stages).

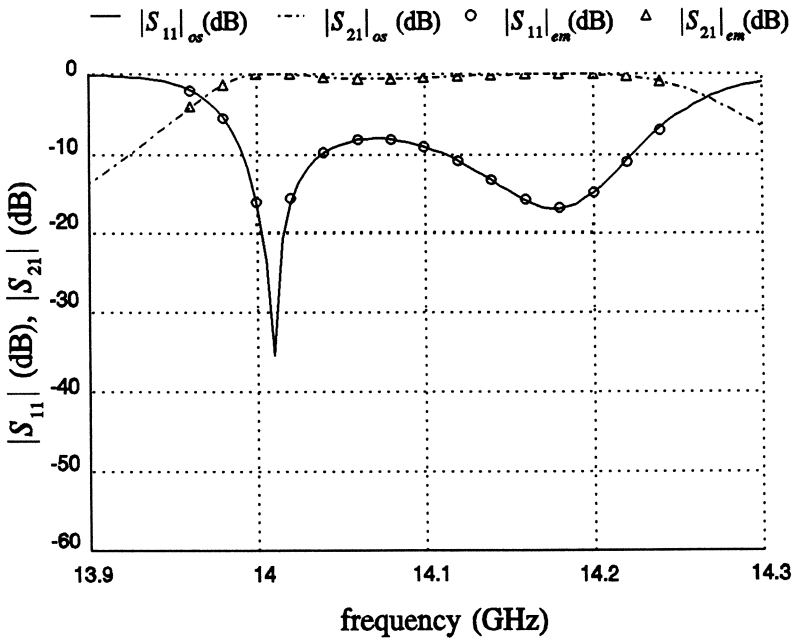

Figure 12. MM responses corresponding to a cluster of 15 points obtained after statistical parameter extraction. The 15 responses are indistinguishable from each other. The match to the FEM response is very good.

yields 100% success (Fig. 13c). The corresponding responses at the solutions are shown in Figure 14. Note that for this case of using $|S_{21}|$ in error definition, starting from the default point, x^*_{os}, yields the correct result. This explains the flawless SM iterations reported in Section III.

The use of $|S_{11}|$ in decibels amplifies errors in the computed parameter S_{11}. The relative error for this case is higher because $|S_{11}|$ is small in the passband region. We have shown that even for such numerically sensitive cases, our new procedure yields successful parameter extractions.

VII. MULTIPOINT PARAMETER EXTRACTION

We used the two-section waveguide transformer example [15] to further investigate the impact of parameter extraction uniqueness on the convergence of the SM iterations. We observed symmetrical ℓ_1 contours with respect to the two section lengths L_1 and L_2, as illustrated in Figure 15, with two local minima. Consequently the result of parameter extraction is not unique. The impact can be seen in the trace depicted in Figure 16, where the SM steps oscillate around the solution due to the "fuzzy" results of parameter extraction.

We introduce a multipoint parameter extraction approach to sharpen the parameter extraction result. Instead of minimizing

$$\|\boldsymbol{R}_{os}(\boldsymbol{x}^i_{os}) - \boldsymbol{R}_{em}(\boldsymbol{x}^i_{em})\| \tag{5}$$

at a single point, we find $\boldsymbol{x}^i_{os}$ by minimizing

$$\|\boldsymbol{R}_{os}(\boldsymbol{x}^i_{os} + \Delta\boldsymbol{x}) - \boldsymbol{R}_{em}(\boldsymbol{x}^i_{em} + \Delta\boldsymbol{x})\|, \tag{6}$$

where $\Delta\boldsymbol{x}$ represents a small perturbation to $\boldsymbol{x}^i_{os}$ and $\boldsymbol{x}^i_{em}$. By simultaneously minimizing (6) with a selected set of $\Delta\boldsymbol{x}$, we hope to improve the uniqueness of the parameter extraction process. Conceptually, we are attempting to match not only the response, but also a first-order change in the response with respect to small perturbations in the parameter values. We have exploited a similar concept in multicircuit modeling [16]. Figure 17 depicts the ℓ_1 contours for multipoint parameter extraction of the two-section transformer, which indicate a unique solution. We used three points (i.e., original $\boldsymbol{x}^i_{em}$ and two perturbations in the L_1 and L_2 directions) for pa-

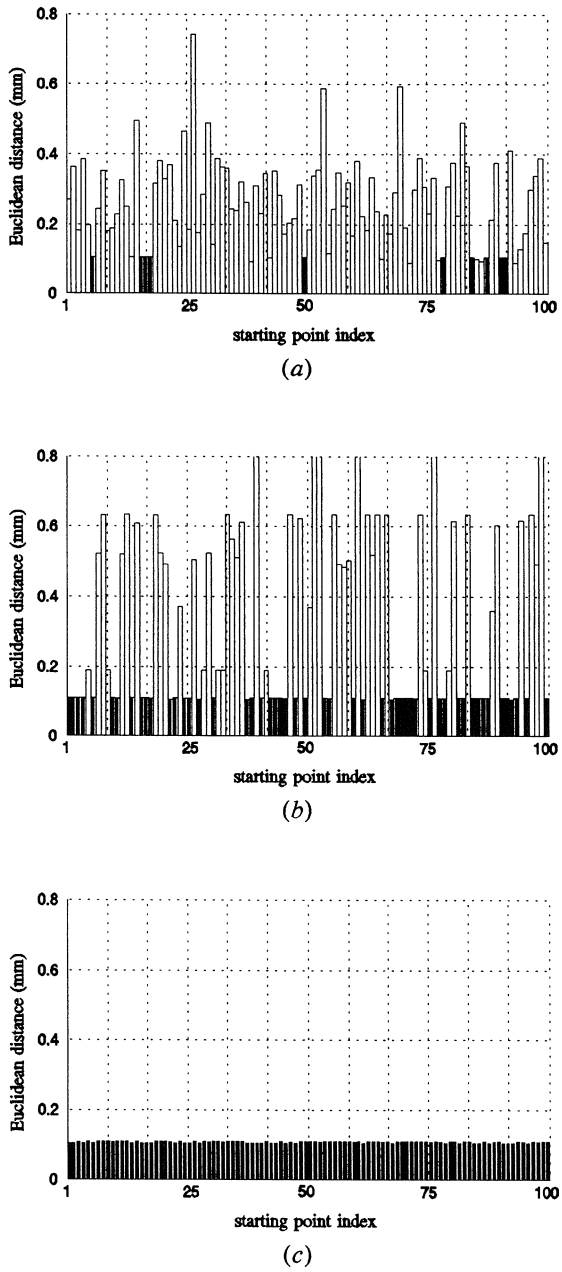

Figure 13. Euclidean distances measured from x_{os}^* to the solution points after the second stage of statistical parameter extraction. (a) Errors defined in terms of $|S_{11}|$ in decibels; no penalty term used. (b) Errors defined in terms of $|S_{21}|$; no penalty term used. (c) Errors defined in terms of $|S_{21}|$; the penalty term (4) used.

rameter extraction. The corresponding SM trace is shown in Figure 18, where the convergence of the SM iterations is dramatically improved. The price we may have to pay for such an improvement is the increased number of X_{em} simulations required: although more X_{em} model simulations are needed in parameter extraction, the overall number of iterations may be reduced.

VIII. TOLERANCE SIMULATION USING SPACE MAPPING

Once the SM is established, it provides not only the design solution (parameter values), but also an efficient means for modeling the circuit in the vicinity of the solution, in particular, for statistical analysis. We can map parameter spreads in the X_{em} space to the corresponding incremental changes in the X_{os} space. Consequently, using the space-mapped X_{os} model, we can rapidly estimate the effects of tolerances, benefitting at the same time from the accuracy of the X_{em} model.

As an illustration, consider Monte Carlo analysis of the H-plane filter using FEM as the X_{em} model and the hybrid MM/network theory simulations as the X_{os} model (Section III). Parameter values are assumed to be normally distributed with a standard deviation of 0.0333% (on the order of 1 μm). The results of Monte Carlo analysis are shown in Figure 19. For a specification on $|S_{11}| < -15$ dB in the passband, the yield, estimated from 200 outcomes, is 88.5%. When the standard deviation is increased to 0.1%, the yield drops to 19% for 200 outcomes. The CPU time required for the entire Monte Carlo analysis with 200 outcomes is comparable to just a single full FEM simulation.

IX. SPACE MAPPING OPTIMIZATION USING COARSE AND FINE MM MODELS

To illustrate the flexibility in selecting the X_{em} and X_{os} models, consider SM between two hybrid MM/network theory models: a coarse model using very few modes and a fine model using many modes to represent the discontinuities. These two models are applied here to optimize waveguide transformers, specifically three- and seven-section transformers described in [15]. In this application, SM enhances the efficiency of the MM-based optimization.

Sharp corners are assumed here, which make the MM models with large numbers of modes very accurate. The RWGMM library allows the designer to implicitly control the number of higher-order modes that are used to model wave-

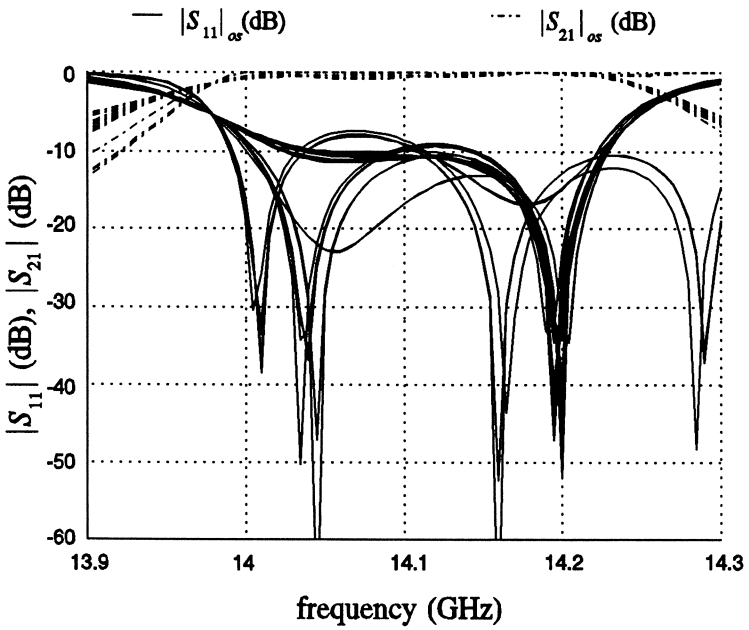

Figure 14. Statistical parameter extraction: responses at 100 solution points (after two stages) corresponding to Figure 13b when no penalty term is used and individual errors are defined in terms of $|S_{21}|$.

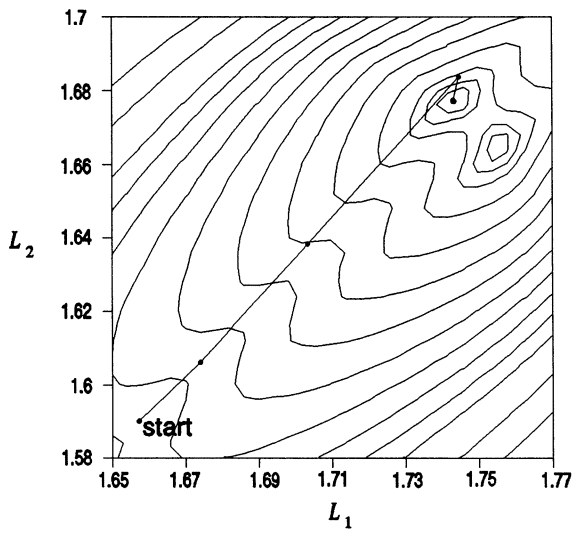

Figure 15. The ℓ_1 contours of the parameter extraction problem for the two-section waveguide transformer. The symmetry between the variables L_1 and L_2 produces two local minima. Consequently, the result of parameter extraction is not unique.

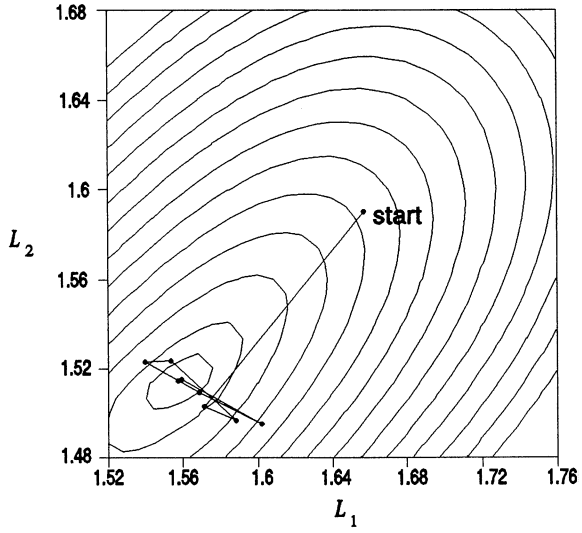

Figure 16. Trace of the SM steps of the two-section waveguide transformer projected onto the minimax contours in the L_1-L_2 plane. The nonunique parameter extraction results lead to the SM steps oscillating around the solution.

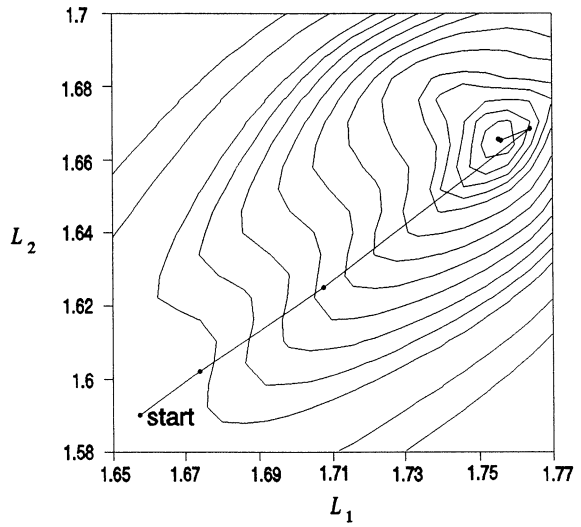

Figure 17. The ℓ_1 contours of multipoint parameter extraction of the two-section waveguide transformer. The parameter extraction has a unique solution.

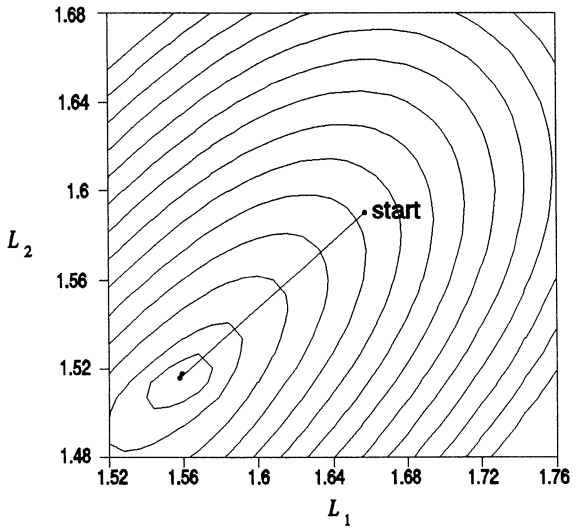

Figure 18. Trace of the SM optimization with multipoint parameter extraction of the two-section transformer projected onto the minimax contours in the L_1-L_2 plane. The convergence is dramatically improved when compared with Figure 16.

guide transition components. Increasing the number of modes improves accuracy at the expense of higher computational cost.

For the coarse model, we use just one mode. For the fine model, we include all the modes below the cutoff frequency of 50 GHz. The actual number of modes included in the fine model is automatically determined by the RWGMM program. As the lengths and heights of the waveguide sections are optimized, the number of modes included in the fine model varies from 49 to 198 for the three-section and at least 180 for the seven-section transformer. The optimized solutions shown in Figures 20 and 21 require 2 and 14 SM iterations, respectively.

X. CONCLUSIONS

We have presented new applications of aggressive space mapping to filter optimization using net-

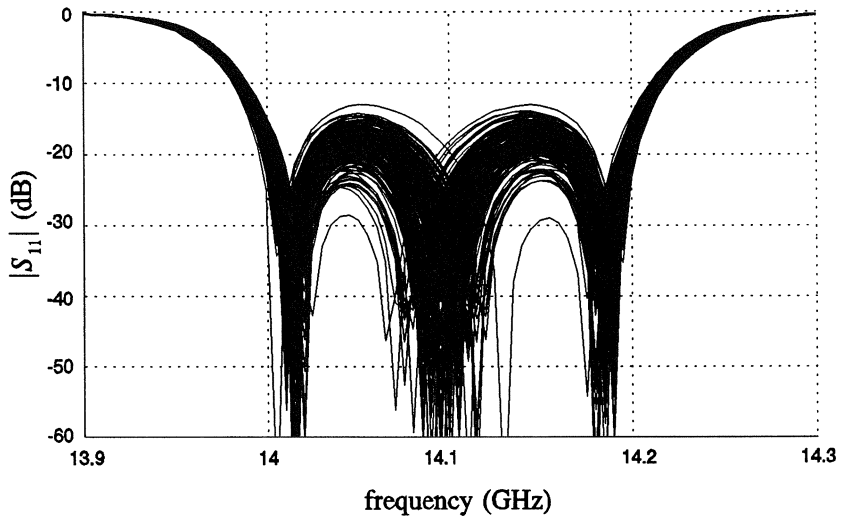

Figure 19. Monte Carlo analysis of the H-plane filter. The parameter values are randomly generated from a normal distribution with a standard deviation of 0.0333%. The yield, estimated from 200 outcomes, is 88.5%.

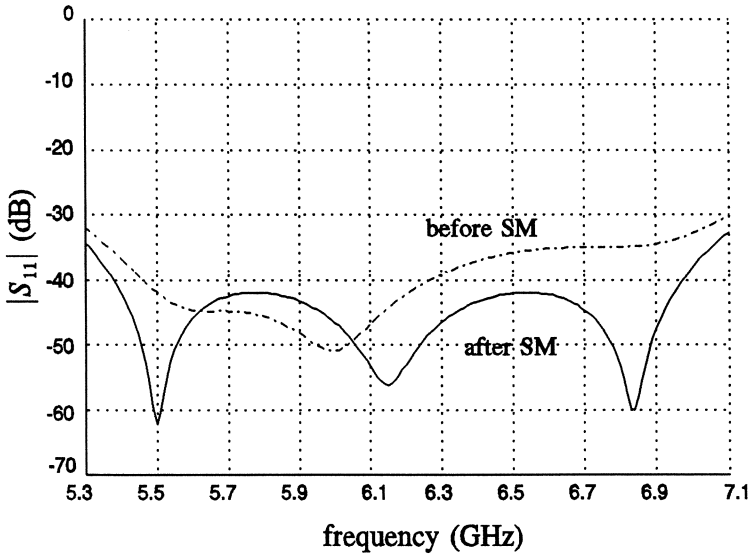

Figure 20. $|S_{11}|$ (in dB) of a three-section waveguide transformer simulated by the RWGMM library before and after two SM iterations. The solution is indistinguishable from the optimal coarse model response.

work theory, mode-matching, and finite element simulation techniques. A statistical approach to parameter extraction incorporating the ℓ_1 error and penalty function concepts has effectively addressed the requirement of a unique and consistent solution. We have introduced a multipoint approach to enhancing the prospect of a unique parameter extraction solution in the space mapping process. SM provides a feasible means for Monte Carlo analysis of microwave circuits that could be carried out with the accuracy of FEM simulations. We have also demonstrated SM optimization based on coarse and fine MM models with different numbers of modes.

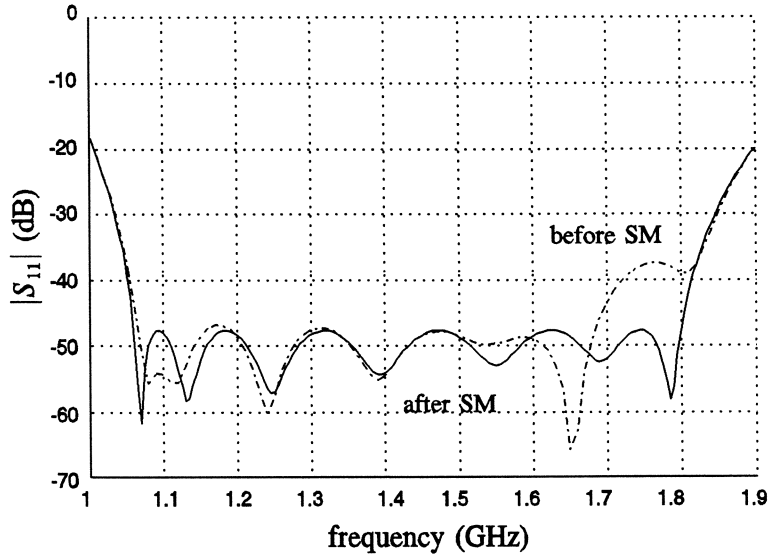

Figure 21. $|S_{11}|$ (in dB) of a seven-section waveguide transformer simulated by the RWGMM library before and after 14 SM iterations. The solution is indistinguishable from the optimal coarse model response.

ACKNOWLEDGMENT

The authors thank HP EEsof Division of Santa Rosa, CA, Ansoft Corp. of Pittsburgh, PA, and Prof. Fritz Arndt of the University of Bremen, Germany, for making their respective software available for this work. This work was carried out and supported in part by Optimization Systems Associates Inc., before acquisition by HP EEsof, and supported in part by the Natural Sciences and Engineering Research Council of Canada under Grants OGP0007239, OGP0042444, and STR0167080, through the Micronet Network of Centres of Excellence and through an Industrial Research Fellowship granted to Dr. Omeragić.

REFERENCES

1. J.W. Bandler, R.M. Biernacki, S.H. Chen, L.W. Hendrick, and D. Omeragić, Electromagnetic optimization of 3D structures, IEEE Trans Microwave Theory Tech 45 (1997), 770–779.
2. F. Arndt, S.H. Chen, W.J.R. Hoefer, N. Jain, R.H. Jansen, A.M. Pavio, R.A. Pucel, R. Sorrentino, and D.G. Swanson, Jr., Automated circuit design using electromagnetic simulators, Workshop WMFE (J. W. Bandler and R. Sorrentino, Organizers and Chairmen), IEEE MTT-S Int. Microwave Symp., Orlando, FL, May 1995.
3. J.W. Bandler, R.M. Biernacki, and S.H. Chen, Fully automated space mapping optimization of 3D structures, IEEE MTT-S Int. Microwave Symp. Dig., San Francisco, CA, June 1996, pp. 753–756.
4. J.W. Bandler, R.M. Biernacki, S.H. Chen, P.A. Grobelny, and R.H. Hemmers, Space mapping technique for electromagnetic optimization, IEEE Trans Microwave Theory Tech 42 (1994), 2536–2544.
5. J.W. Bandler, R.M. Biernacki, S.H. Chen, R.H. Hemmers, and K. Madsen, Electromagnetic optimization exploiting aggressive space mapping, IEEE Trans Microwave Theory Tech 43 (1995), 2874–2882.
6. T. Sieverding, U. Papziner, T. Wolf, and F. Arndt, New mode-matching building blocks for common circuit CAD programs, Microwave J, 36 (1993), 66–79.
7. F. Arndt, T. Sieverding, T. Wolf, and U. Papziner, Optimization-oriented design of rectangular and circular waveguide components using efficient mode-matching simulators in commercial circuit CAD tools, Int J Microwave Millimeter-Wave CAE 7 (1997), 37–51.
8. F. Alessandri, M. Dionigi, and R. Sorrentino, A fullwave CAD tool for waveguide components using a high speed direct optimizer, IEEE Trans Microwave Theory Tech 43 (1995), 2046–2052.
9. P.P. Silvester and G. Pelosi, Finite elements for wave electromagnetics, methods and techniques, IEEE Press, New York, 1994.
10. J.-F. Lee, D.-K. Sun, and Z.J. Cendes, Full-wave analysis of dielectric waveguides using tangential vector finite elements, IEEE Trans Microwave Theory Tech 39 (1991), 1262–1271.
11. J.W. Bandler, R.M. Biernacki, S.H. Chen, and P. A. Grobelny, Optimization technology for nonlinear microwave circuits integrating electromagnetic simulations, Int J Microwave Millimeter-Wave CAE 7 (1997), 6–28.
12. F. Arndt, Microwave Department, University of Bremen, private communications.
13. J.W. Bandler, S.H. Chen, and S. Daijavad, Microwave device modeling using efficient l_1 optimization: a novel approach, IEEE Trans Microwave Theory Tech MTT-34 (1986), 1282–1293.
14. J.W. Bandler, R.M. Biernacki, S.H. Chen, and Y.F. Huang, Design optimization of interdigital filters using aggressive space mapping and decomposition, IEEE Trans. Microwave Theory Tech 45 (1997), 761–769.
15. J.W. Bandler, Computer optimization of inhomogeneous waveguide transformers, IEEE Trans Microwave Theory Tech MTT-17 (1969), 563–571.
16. J.W. Bandler and S.H. Chen, Circuit optimization: the state of the art, IEEE Trans Microwave Theory Tech 36 (1988), 424–443.

BIOGRAPHIES

John W. Bandler was born in Jerusalem, on November 9, 1941. He studied at Imperial College of Science and Technology, London, England, from 1960 to 1966. He received the B.Sc. (Eng.), Ph.D., and D.Sc. (Eng.) degrees from the University of London, London, England, in 1963, 1967, and 1976, respectively. He joined Mullard Research Laboratories, Redhill, Surrey, England in 1966. From 1967 to 1969 he was a postdoctoral fellow and sessional lecturer at the University of Manitoba, Winnipeg, Canada. Dr. Bandler joined McMaster University, Hamilton, Canada, in 1969, where he is currently a professor of electrical and computer engineering. He has served as Chairman of the Department of Electrical Engineering and Dean of the Faculty of Engineering. He currently directs research in the Simulation Optimization Systems Research Laboratory.

Dr. Bandler has pioneered contributions in simulation, sensitivity analysis, and optimization of linear and nonlinear circuits, statistical design centering, design with tolerances and postproduction tuning, yield-driven design optimization, fault

diagnosis of analog circuits, optimal load flow in power systems, GaAs device statistical modeling, and parameter extraction.

He was President of Optimization Systems Associates Inc. (OSA), which he founded in 1983, until November 20, 1997, the date when OSA was acquired by Hewlett-Packard Company (HP). OSA implemented a first-generation yield-driven microwave CAD capability for Raytheon in 1985, followed by further innovations in linear and nonlinear microwave CAD technology for the Raytheon/Texas Instruments Joint Venture MIMIC Program. OSA introduced the CAE systems RoMPE™ in 1988, HarPE™ in 1989, OSA90™ and OSA90/hope™ in 1991, Empipe™ in 1992, and Empipe3D™ and EmpipeExpress™ in 1996. OSA created the product ***empath***™ in 1996, which was marketed by Sonnet Software, Inc. Dr. Bandler is President of Bandler Corporation, which he founded in 1997.

Dr. Bandler was an Associate Editor of the *IEEE Transactions on Microwave Theory and Techniques* (1969–1974) and has continued serving as a member of the Editorial Board. He was Guest Editor of the special issue of the *IEEE Transactions on Microwave Theory and Techniques* on computer-oriented microwave practices (1974) and Guest Co-Editor with Rolf H. Jansen of the special issue of the *IEEE Transactions on Microwave Theory and Techniques* on process-oriented microwave CAD and modeling (1992). He joined the Editorial Boards of the *International Journal of Numerical Modelling* in 1987, and the *International Journal of Microwave and Millimeterwave Computer-Aided Engineering* in 1989. He was Guest Editor of the special issue of *International Journal of Microwave and Millimeter-Wave Computer-Aided Engineering*, on optimization-oriented microwave CAD (1997) and Guest Editor of the special issue of *IEEE Transactions on Microwave Theory and Techniques* on automated circuit design using electromagnetic simulators (1997).

Dr. Bandler published more than 300 papers between 1965 and 1998. He contributed to *Modern Filter Theory and Design*, Wiley-Interscience (1973) and to *Analog Methods for Computer-Aided Analysis and Diagnosis*, Marcel Dekker, Inc. (1988). Four of his papers have been reprinted in *Computer-Aided Filter Design*, IEEE Press (1973), one in each of *Microwave Integrated Circuits*, Artech House (1975), *Low-Noise Microwave Transistors and Amplifiers*, IEEE Press (1981), *Microwave Integrated Circuits*, 2nd ed., Artech House (1985), *Statistical Design of Integrated Circuits*, IEEE Press (1987), and *Analog Fault Diagnosis*, IEEE Press (1987).

Dr. Bandler is a Fellow of the Royal Society of Canada, a Fellow of the Institute of Electrical and Electronics Engineers, a Fellow of the Institution of Electrical Engineers (Great Britain), a Member of the Association of Professional Engineers of the Province of Ontario (Canada), and a Member of the MIT Electromagnetics Academy. He is a member of the Micronet Network of Centres of Excellence. He received the Automatic Radio Frequency Techniques Group (ARFTG) Automated Measurements Career Award in 1994.

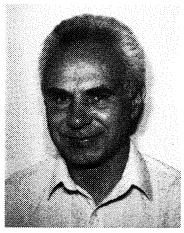

Radoslaw M. Biernacki was born in Warsaw, Poland. He received the Ph.D. degree from Warsaw University of Technology, Warsaw, Poland, in 1976. He became a research and teaching assistant in 1969 and an assistant professor in 1976 at the Institute of Electronics Fundamentals, Warsaw University of Technology, Warsaw, Poland. From 1978 to 1980 he was on leave with the Research Group on Simulation, Optimization and Control and with the Department of Electrical and Computer Engineering at McMaster University, Hamilton, Canada, as a postdoctoral fellow. From 1984 to 1986 he was a visiting associate professor at Texas A & M University, College Station, TX. From 1986 to 1997 he was with Optimization Systems Associates Inc., Dundas, Ontario, Canada, where he was involved in the development of OSAs commercial CAE software systems and related research. In 1997, after acquisition of OSA, he joined the R & D team of HP EEsof. Dr. Biernacki's research in the area of computer-aided engineering has included parameter extraction, statistical device modeling, simulation and optimization, yield-driven design of linear and nonlinear microwave circuits, and electromagnetic design optimization. He has more than 100 publications and is a Fellow of the Institute of Electrical and Electronics Engineers. He is also an adjunct professor in the Department of Electrical and Computer Engineering at McMaster University, Hamilton, Canada.

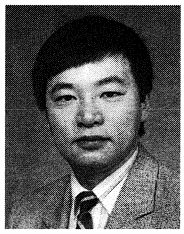

Shao Hua (Steve) Chen was born in Swatow, China, He received the B.S. (Eng.) degree in 1982 from the South China Institute of Technology in Guangzhou, China, and the Ph.D. degree in electrical engineering in 1987 from McMaster University in Hamilton, Canada.

From July 1982 to August 1983 he was a teaching assistant in the Department of Automation at the South China Institute of Technology. During his graduate study at McMaster University from 1983 to 1987, he was awarded an Ontario Graduate Scholarship for two years. He joined Optimization Systems Associates Inc., in Dundas, Ontario, Canada, in 1987 and has made major contributions to the commercial CAD software development. He has also worked as a senior research engineer in the Simulation Optimization Systems Research Laboratory at McMaster University and engaged in pioneering research on CAD simulation and modeling technology and optimization techniques. In 1997, he joined the technical staff at Hewlett-Packard Company, HP EEsof Division. His professional interests include optimization theory and implementation, CAD software architecture, electromagnetic optimization, electronic device modeling, statistical circuit simulation, and computer graphics. He has authored over 60 technical publications.

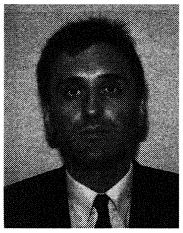

Dževat Omeragić received the Dipl.-Ing. and M.Eng. degree in electrical engineering from the University of Sarajevo, Bosnia-Herzegovina, in 1986 and 1990, respectively, and a Ph.D. from McGill University, Montreal, Canada, in January 1994.

From 1986 to 1990 he was a research engineer and assistant with the Department of Electrical Engineering of Sarajevo University, working in CAD in electrical power engineering, electromagnetic transients in HV networks, and electric and magnetic field computation. He joined the Computational Analysis and Design Laboratory and the Department of Electrical Engineering at McGill University as a graduate student in 1990. He held an NSERC WUSC Fellowship for the academic year

1990–1991. From 1994 to 1996 he was a postdoctoral fellow and research associate at McGill University, doing research in the area of finite element methods and CAD postprocessing. He joined the Simulation Optimization Systems Research Laboratory and the Department of Electrical and Computer Engineering at McMaster University, Hamilton, Canada, in April 1996, as a research engineer working on EM optimization. He also spent three months with Optimization Systems Associates Inc. (now part of HP EEsof Division) as an NSERC industrial research fellow, working on space mapping optimization. Since April 1997, Dr. Omeragic has been with the Schlumberger Oilfield Services, Sugar Land Product Center, Sugar Land, TX, working in the area of EM modeling and inversion for well logging applications. His research interests include computational electromagnetics, optimization, and inverse problems.

Dr. Omeragic is a member of the IEEE, SPWLA, and SPE.